CHEMISTRY OF MATERIALS
Article

Chem. Mater. **2010,** *22,* 3269–3276 3269
DOI:10.1021/cm100578u

Frustrated and Unfrustrated Magnetic Orders in the 10H Perovskite $Ba_5Sb_{1-x}Mn_{4+x}O_{15-\delta}$

Congling Yin,[†,‡] Guobao Li,*[,†] Winfried A. Kockelmann,[§] Fuhui Liao,[†] J. Paul Attfield,*[,‡] and Jianhua Lin*[,†]

[†]*Beijing National Laboratory for Molecular Sciences, State Key Laboratory of Rare Earth Materials Chemistry and Applications, College of Chemistry and Molecular Engineering, Peking University, Beijing 100871, P. R. China,* [‡]*Centre for Science at Extreme Conditions and School of Chemistry, University of Edinburgh, King's Building, Mayfield Road, Edinburgh, U.K. EH9 3JZ, and* [§]*ISIS Facility, Rutherford Appleton Laboratory, Chilton, U.K.*

Received February 25, 2010. Revised Manuscript Received April 8, 2010

A 10-layer hexagonal perovskite $Ba_5Sb_{1-x}Mn_{4+x}O_{15-\delta}$ solid solution ($0.24 \le x \le 0.36$; space group $P6_3/mmc$, $a = 5.7095(1)$ Å, and $c = 23.4866(3)$ Å for $x = 0.36$) has been synthesized by solid state reaction and studied using powder X-ray and neutron diffraction and magnetization measurements. This 10H polytype structure contains one corner-sharing $(Sb,Mn)O_6$ octahedron and a tetramer of four face-sharing MnO_6 octahedra per formula unit. Two magnetic transitions are observed at 129−167 K (T_M) and 13−22 K (T_F). The frustration index $|\theta|/T_M$, where θ is the Weiss temperature, is very close to unity, but considerable magnetic frustration is evidenced through the long-range order of a small $\sim 0.5\ \mu_B$ antiferromagnetic moment below T_M, and the formation of ferro- or ferrimagnetic clusters. These freeze at T_F with the $|\theta|/T_F \approx 7-10$ index representing high magnetic frustration. T_F increases directly with the excess of Mn, x, in $Ba_5Sb_{1-x}Mn_{4+x}O_{15-\delta}$ rather than with the overall Mn content, showing that the occupation of the corner-sharing Sb/Mn sites is key to the extended magnetism.

1. Introduction

Interest in the physics of manganites has led to the investigation of other, hexagonal, perovskites such as $BaMnO_{3-y}$ which shows a rich variety of structural and magnetic properties.[1−5] A series of $BaMnO_{3-y}$ polytypes (2H → 15R → 8H → 6H → 10H → 4H; this notation shows the number of closely packed layers in the repeat sequence and the lattice symmetry as H for hexagonal and R for rhombohedral) have been identified as the oxygen vacancy concentration y increases.[4,5] Further perovskite polytypes may be generated when Mn is substituted with other cations.

Many doped $BaMn_{1-x}M_xO_3$ systems have been explored, for example, with M = Ti,[6] Ca,[7,8] Ir,[9] rare earths,[10−14] In,[15,16] Co,[17,18] Ru,[19] and Fe.[20] This led to the discovery of a new series of M cation ordered 10H perovskites $Ba_5In_{0.93}Mn_4O_{14.40}$[15] and $Ba_5Sn_{1.1}Mn_{3.9}O_{15}$,[21] which contain one corner-sharing MO_6 octahedron and a tetramer of four face-sharing MnO_6 octahedra. Magnetization measurements showed that these materials are paramagnetic with antiferromagnetic interactions between Mn spins, but no magnetic order was observed down to 2 K. Here we report the synthesis, structural characterization, and magnetic properties of a new 10H solid solution, $Ba_5Sb_{1-x}Mn_{4+x}O_{15}$ ($0.24 \le x \le 0.36$), in which partial occupancy of Mn at the

*To whom correspondence should be addressed. E-mail: liguobao@pku.edu.cn, j.p.attfield@ed.ac.uk, and jhlin@pku.edu.cn.

(1) Gonzalez-Calbet, J. M.; Parras, M.; Alonso, J. M.; Vallet-Regi, M. *J. Solid State Chem.* **1993**, *106*, 99.
(2) Negas, T.; Roth, R. S. *J. Solid State Chem.* **1971**, *3*, 323.
(3) Cussen, E. J.; Battle, P. D. *Chem. Mater.* **2000**, *12*, 831.
(4) Adkin, J. J.; Hayward, M. A. *Chem. Mater.* **2007**, *19*, 755.
(5) Adkin, J. J.; Hayward, M. A. *J. Solid State Chem.* **2006**, *179*, 70.
(6) Keith, G. M.; Kirk, C. A.; Sarma, K.; Alford, N. M.; Cussen, E. J.; Rosseinsky, M. J.; Sinclair, D. C. *Chem. Mater.* **2004**, *16*, 2007.
(7) Floros, N.; Michel, C.; Hervieu, M.; Raveau, B. *J. Solid State Chem.* **2002**, *168*, 11.
(8) Floros, N.; Michel, C.; Hervieu, M.; Raveau, B. *Chem. Mater.* **2000**, *12*, 3197.
(9) Jordan, N. A.; Battle, P. D. *J. Mater. Chem.* **2003**, *13*, 2220.
(10) Yang, H.; Cao, Z. E.; Shen, X.; Feng, W. J.; Jiang, J. L.; Dai, J. F.; Yu, R. C. *J. Mater. Sci.* **2008**, *43*, 5679.
(11) Yang, H.; Tang, Y. K.; Yao, L. D.; Zhang, W.; Li, Q. A.; Li, F. Y.; Jin, C. Q.; Yu, R. C. *J. Alloys Compd.* **2007**, *432*, 283.
(12) Kuang, X. J.; Bridges, C.; Allix, M.; Claridge, J. B.; Hughes, H.; Rosseinsky, M. J. *Chem. Mater.* **2006**, *18*, 5130.
(13) Fuentes, A. F.; Boulahya, K.; Amador, U. *J. Solid State Chem.* **2004**, *177*, 714.
(14) Rabbow, C.; Mullerbuschbaum, H. *Z. Naturforsch., B: Chem. Sci.* **1994**, *49*, 1277.
(15) Yin, C.; Li, G.; Jin, T.; You, L.; Tao, J.; Richardson, J. W.; Loong, C. K.; Sun, J.; Liao, F.; Lin, J. *Chem. Mater.* **2008**, *20*, 2110.
(16) Creon, N.; Michel, C.; Hervieu, A.; Maignan, A.; Raveau, B. *Solid State Sci.* **2003**, *5*, 243.
(17) Miranda, L.; Feteira, A.; Sinclair, D. C.; Hernandez, M. G.; Boulahya, K.; Hernando, M.; Varela, A.; Gonzalez-Calbet, J. M.; Parras, M. *Chem. Mater.* **2008**, *20*, 2818.
(18) Miranda, L.; Ramirez-Castellanos, J.; Varela, A.; Gonzalez-Calbet, J. M.; Parras, M.; Hernando, M.; Fernandez-Diaz, M. T.; Hernandez, M. G. *Chem. Mater.* **2007**, *19*, 1503.
(19) Yin, C.; Li, G.; Kockelmann, W. A.; Lin, J.; Attfield, J. P. *Phys. Rev. B* **2009**, *80*, 094420.
(20) Miranda, L.; Ramirez-Castellanos, J.; Hernando, M.; Varela, A.; Gonzalez-Calbet, J. M.; Parras, M. *Eur. J. Inorg. Chem.* **2007**, *15*, 2129.
(21) Yin, C.; Li, G.; Jin, T.; Tao, J.; Richardson, J. W.; Loong, C.-K.; Liao, F.; Lin, J. *J. Alloys Compd.* **2010**, *489*, 152.

Published on Web 04/21/2010

corner-sharing octahedral site results in an unusual magnetism. Two magnetic orders are observed, one of which has transition temperatures characteristic of unfrustrated order, while the other corresponds to the freezing of frustrated cluster spins.

2. Experimental Section

Polycrystalline samples of nominal composition $Ba_5Sb_{1-x}Mn_{4+x}O_{15-\delta}$ (nominal $x = 0.16-0.40$) were synthesized from $BaCO_3$ (99.9%), $MnCO_3$ (99.9%), and $SbO_{1.5}$ (99.9%) in a $5:(4+x):1.03(1-x)$ molar ratio. A 3% excess of Sb was used to compensate for the volatility of Sb_2O_3 under reaction conditions. The starting materials were mixed in an agate mortar and pestle and heated in an alumina crucible at 1000 °C for 10 h in air. The sample was reground, pressed into pellets (20 ton/cm^2), heated at 1300 °C for 30 h with several intermediate pressing and grinding steps, and slowly cooled to room temperature.

Samples were characterized by powder X-ray diffraction on a Bruker AXS D8 diffractometer with germanium monochromatized Cu Kα1 radiation at 40 kV and 40 mA. Data were collected in the range of 7−120° in step scanning mode for structural refinement. Neutron diffraction data were collected from the $x = 0.36$ sample on the time-of-flight GEM diffractometer at the ISIS spallation neutron source between 5 and 300 K, to investigate the structure and any magnetic order.

Magnetization measurements for the four $Ba_5Sb_{1-x}Mn_{4+x}O_{15-\delta}$ samples ($0.24 \le x \le 0.36$) were performed using a Quantum Design SQUID magnetometer. Data were recorded in a 1000 Oe field while the samples were warmed from 5 to 300 K, following zero-field cooling (ZFC) or field cooling (FC).

3. Results and Discussion

(a). Structure Refinements. The X-ray patterns of the $Ba_5Sb_{1-x}Mn_{4+x}O_{15-\delta}$ ($x = 0.24-0.36$) samples are similar to that of $Ba_5In_{0.93}Mn_4O_{14.40}$ and can be indexed with the 10H perovskite lattice. Beyond these composition limits, secondary phases are observed, as shown for the nominal $x = 0.16$, 0.20, and 0.40 samples in Figure 1. This indicates that 10H-type $Ba_5Sb_{1-x}Mn_{4+x}O_{15-\delta}$ solid solutions are formed over a narrow range of compositions, nominally $x = 0.24-0.36$. This is confirmed by the systematic decreases in the hexagonal lattice parameters (obtained by Le Bail fits to the X-ray data) and volume with x shown in Figure 2.

The crystal structure of the $x = 0.36$ sample was refined simultaneously against the 300 K powder X-ray and neutron data (Figure 3) using GSAS.[22] The starting model was the reported 10H $Ba_5In_{0.93}Mn_4O_{14.40}$ structure, which has three octahedral cation sites, $M1$, $M2$, and $M3$, as shown in Figure 4. The occupancies of Sb and Mn were initially refined at the $M1$, $M2$, and $M3$ sites with each site sum subject to unity. No significant Sb occupancy was observed at the $M2$ and $M3$ sites, so a variable Mn/Sb occupancy was refined only at the $M1$ site thereafter. Possible oxygen vacancies at the distinct O1, O2, and O3 sites were refined and were found only at the O3 position. In the final refinement, the temperature (U) factors of the $M1$, $M2$, and $M3$ sites were constrained to have identical values. Good fits were obtained, with an overall weighted profile wRp factor of 3.89%, and the X-ray and neutron plots are shown in Figure 3. The refined crystallographic parameters and selected bond lengths and bond angles are listed in Tables 1 and 2, respectively.

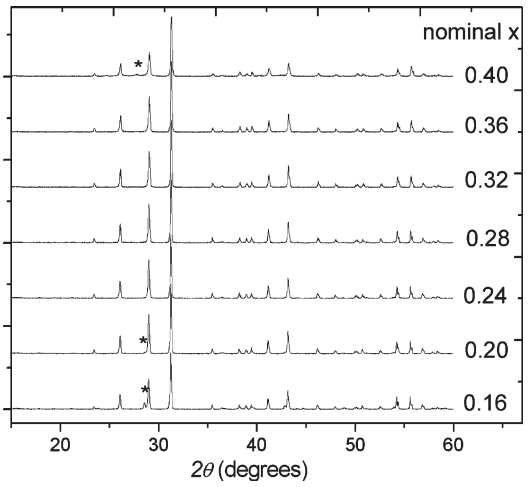

Figure 1. X-ray diffraction patterns of $Ba_5Sb_{1-x}Mn_{4+x}O_{15-\delta}$ with the nominal $x = 0.16-0.40$ compositions. Impurity peaks are observed for $x = 0.16$, 0.20, and 0.40 (marked with an asterisk).

$Ba_5Sb_{0.64}Mn_{4.36}O_{15-\delta}$ adopts a 10H hexagonal perovskite structure (Figure 4), in which hexagonal (h) and cubic (c) closely packed BaO_{3-x} layers stack in the sequence $(chhhc)_2$. This is different from the $(hchch)_2$ stacking observed in 10H $BaMnO_{3-\delta}$. The structure refinement shows that Sb occupies only the $M1$ site, and the refined $x = 0.31$ value is close to the nominal $x = 0.36$ value. BVS (bond valence sum) estimates of the formal M site charges were calculated using standard parameters[23] and a linear interpolation between Mn^{3+} and Mn^{4+} for the Mn sites.[24] The results listed in Table 1 show that the formal Mn charges are segregated, with Sb^{5+} and Mn^{3+} (which have similar ionic radii of 0.60 and 0.645 Å, respectively) at the corner-sharing $M1$ site, mixed Mn^{3+}/Mn^{4+} at the $M2$ site, and Mn^{4+} at the $M3$ site. This corresponds to the chemical formula $Ba_5(Sb1^{5+}{}_{1-x}Mn1^{3+}{}_x)(Mn2^{4+}{}_{0.5+x-\delta}Mn2^{3+}{}_{0.5-x+\delta})_2(Mn3^{4+})_2O_{15-\delta}$, where Mn1 corresponds to Mn at site $M1$, etc. For the refined $x = 0.31$ and $\delta = 0.41$ values, the predicted average charge of +3.4 for Mn2 agrees well with the BVS of 3.5. Oxygen vacancies occur at the O3 site in the hexagonally packed BaO_3 layers, where they are also observed in polymorphs of $BaMnO_{3-y}$.[4,5] The decrease in the lattice parameters and volume with x across the solid solution of $Ba_5Sb_{1-x}Mn_{4+x}O_{15-\delta}$ shown in Figure 2 is in keeping with the substitution of Mn^{4+} (0.53 Å) for the larger Mn^{3+} (0.645 Å) and Sb^{5+} (0.60 Å). The nonlinear behavior probably arises from the changing oxygen vacancy concentrations as a significant $\delta = 0.41$ is observed in the $x = 0.36$ sample.

(22) Larson, A. C.; Von Dreele, R. B. Los Alamos National Laboratory Report LAUR **2004**, pp 86−748 (unpublished).

(23) Brown, I. D.; Altermatt, D. *Acta Crystallogr.* **1985**, *B41*, 244.

(24) Attfield, J. P. *Solid State Sci.* **2006**, *8*, 861.

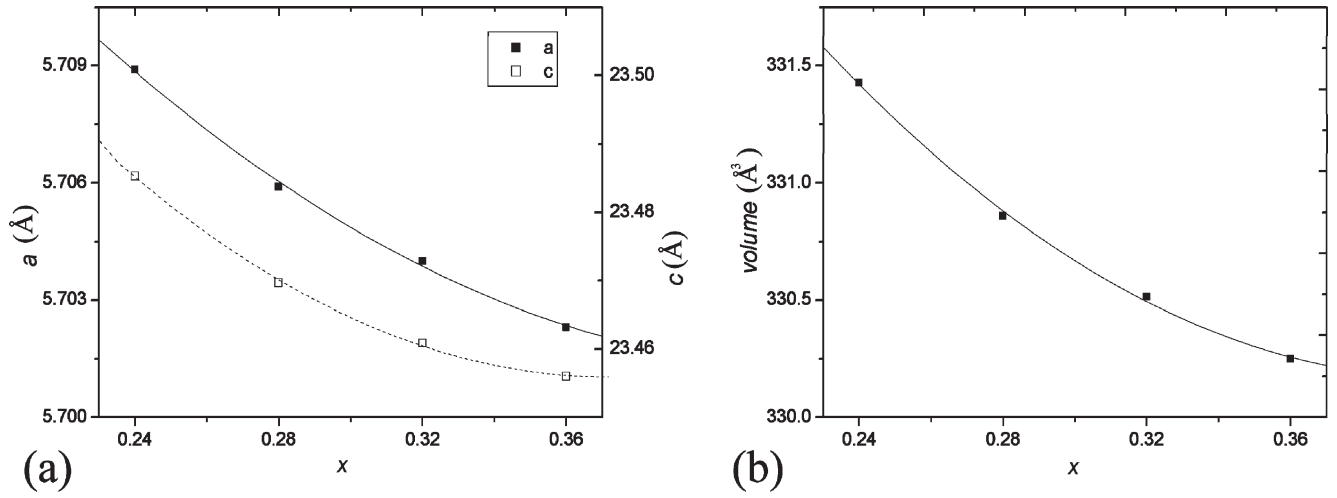

Figure 2. Variation of the (a) lattice parameter and (b) cell volume with the nominal x values across 10H $Ba_5Sb_{1-x}Mn_{4+x}O_{15-\delta}$ solid solutions.

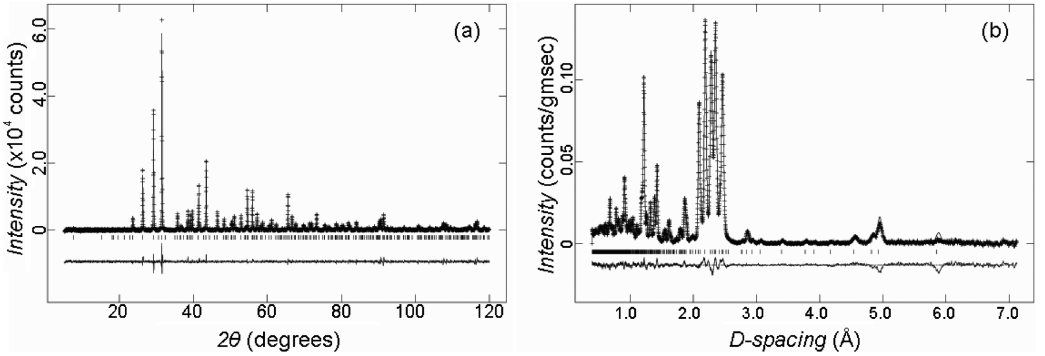

Figure 3. Observed, calculated, and difference plots for the structure refinement of $Ba_5Sb_{0.64}Mn_{4.36}O_{15-\delta}$ at 300 K against (a) X-ray and (b) neutron powder diffraction profiles.

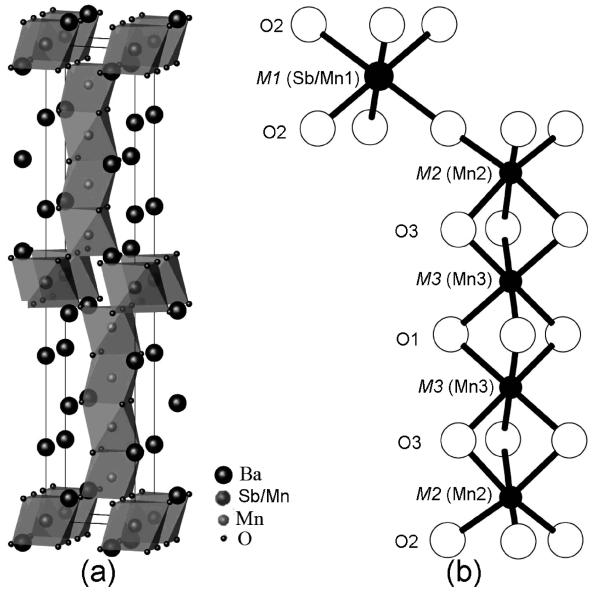

Figure 4. (a) Crystal structure model and (b) detail showing the M cation and O sites for $Ba_5Sb_{1-x}Mn_{4+x}O_{15-\delta}$.

The cation and oxygen vacancy distributions in $Ba_5Sb_{1-x}Mn_{4+x}O_{15-\delta}$ are different from those of the In- and Sn-doped analogues because of the differing sizes and charges of the dopants. In $Ba_5In_{0.93}Mn_4O_{14.40}$, In^{3+} and Mn^{4+} ions are ordered between the corner-sharing ($M1$) and face-sharing ($M2$ and $M3$) octahedral sites, respectively, with indium vacancies, and oxygen vacancies were also found in the c-BaO_3 layers (O2 sites). In $Ba_5Sn_{1.1}Mn_{3.9}O_{15}$, Sn and Mn are disordered over the corner-sharing $M1$ (0.86:0.14 Sn:Mn ratio) and terminal face-sharing $M2$ (0.12:0.88 Sn:Mn ratio) sites, and no oxygen deficiency was observed. In $Ba_5Sb_{0.64}Mn_{4.36}O_{15-\delta}$, the $M1$ site is occupied by Sb and Mn ions, $M2$ and $M3$ sites are occupied by Mn ions, and oxygen vacancies are observed at the O3 site located in the h-BaO_3 layers. The structure of $Ba_5Sb_{0.64}Mn_{4.36}O_{15-\delta}$ contains a higher proportion of magnetic cations (31% Mn) at the $M1$ sites that interconnect the Mn_4O_{15} tetramers of face-sharing octahedra, which has a strong impact on the magnetic properties as discussed below.

(b). Magnetic Properties. Magnetization measurements for the four $Ba_5Sb_{1-x}Mn_{4+x}O_{15-\delta}$ samples ($0.24 \leq x \leq 0.36$) are shown in Figure 5. All of the samples are paramagnetic at high temperatures, and the susceptibilities from 200 to 300 K are fitted well by a Curie−Weiss law, giving the paramagnetic moments (μ_{eff}) and Weiss temperatures (θ) listed in Table 3. The negative θ values show that the dominant exchange interactions are antiferromagnetic.

Two intrinsic spin ordering transitions are evident in $Ba_5Sb_{1-x}Mn_{4+x}O_{15-\delta}$. A high-temperature transition is

Table 1. Refined Atomic Parameters for $Ba_5Sb_{0.64}Mn_{4.36}O_{15-\delta}$ in Space Group $P6_3/mmc$ at 300 K[a]

atom	site	*x*, *y*, *z*	occupancy	*U* (Å^2)	BVS
Ba1	2d	$^2/_3$, $^1/_3$, $^1/_4$	1	0.0065(4)	
Ba2	4f	$^2/_3$, $^1/_3$, 0.4445(1)	1	0.0024(3)	
Ba3	4e	0, 0, 0.3455(1)	1	0.0068(3)	
*M*1 (Sb/Mn1)	2a	0, 0, $^1/_2$	0.686(3)/0.314(3)	0.0052(2)	4.94/2.96
*M*2 (Mn2)	4f	$^1/_3$, $^2/_3$, 0.4072(1)	1	0.0052(2)	3.50
*M*3 (Mn3)	4f	$^1/_3$, $^2/_3$, 0.3018(1)	1	0.0052(2)	3.85
O1	6h	0.1834(1), 0.8166(1), 0.25	1	0.0042(2)	
O2	12k	0.1675(1), 0.3349(2), 0.4512(3)	1	0.0068(1)	
O3	12k	0.4811(1), 0.9623(2), 0.3528(3)	0.931(2)	0.0046(2)	

[a] Lattice parameters are as follows: $a = 5.7095(1)$ Å, and $c = 23.4866(3)$ Å; volume $V = 663.06(2)$ Å^3. Bond valence sum (BVS) estimates of the formal *M* site charges are calculated using parameters for Sb^{5+} and for linear interpolation between Mn^{3+} and Mn^{4+}.

Table 2. Bond Lengths and Angles for $Ba_5Sb_{0.64}Mn_{4.36}O_{15-\delta}$ at 300 K

bond length (Å)	bond length (Å)	bond angle (deg)
Sb/Mn1−O2 (×6), 2.0133(7)	Mn3−O3 (×3), 1.8855(12)	Sb/Mn1−O2−Mn2, 177.49(6)
Mn2−O2 (×3), 1.9373(12)	Mn2−Mn3, 2.4731(22)	Mn2−O3−Mn3, 80.47(5)
Mn2−O3 (×3), 1.9438(14)	Mn3−Mn3, 2.4409(33)	Mn3−O1−Mn3, 78.92(9)
Mn3−O1 (×3), 1.9202(14)		

evident from the change in the slope of susceptibility or inverse susceptibility at 130−170 K (T_M). This transition becomes sharper as *x* increases. The enhanced susceptibility below T_M shows that ferromagnetic correlations are present, and the lack of divergence between ZFC and FC data indicates that the correlations are dynamic. A jump in the susceptibility and divergence of ZFC and FC data below 42 K is seen for all samples, but this is characteristic of a trace of the ferromagnetic phase Mn_3O_4, below the limit of detection by X-ray diffraction. A further, intrinsic ZFC−FC divergence and a discontinuity or peak in the ZFC susceptibilities mark the second, spin freezing transition when $T_F < 25$ K. Such freezing transitions are observed in other hexagonal manganese oxide perovskites at similar temperatures.[12,25] Both magnetic transition temperatures T_M and T_F increase rapidly with the excess Mn content *x*, as shown in Figure 6. The freezing transition shows an approximate $T_F \propto x$ variation, and the T_M values are close to the magnitude of the Weiss temperature (Table 3). The μ_{eff} values are in the range of 3.50−3.76 μ_B, which is comparable to the spin-only paramagnetic moment for Mn^{4+} (3.87 μ_B). These are lower than the values predicted from spin-only behavior; for example, the value expected from the above cation and charge distribution in the $x = 0.36$ sample is 4.26 μ_B.

The low-temperature neutron diffraction patterns of the $Ba_5Sb_{0.64}Mn_{4.36}O_{15-\delta}$ sample were used to determine whether any long-range magnetic order occurs below transitions T_M and T_F. The only observed magnetic diffraction intensity is the very weak (005) peak, as shown in Figure 7. At low temperatures, this is comparable in width to the nuclear diffraction peaks and is therefore evidence of long-range spin order. The peak is too weak to enable meaningful intensity and width variations with temperature to be determined independently, but the intensity variation assuming that the peak width remains the same as that of the nuclear peaks is shown in Figure 7. This demonstrates that the ordering transition is above 100 K and so does not correspond to T_F, and we therefore conclude that this magnetic order occurs below T_M. A dominant (005) magnetic peak is expected for this 10H structure when layers of parallel moments lie in the *a*−*b* plane and are antiferromagnetically coupled to adjacent planes. This is consistent with spin ordering models such as those shown in Figure 8, and a fit of the arrangement in Figure 8b to the 5 K neutron data accounts for the (005) magnetic peak without predicting other significant magnetic intensities (Figure 9). The ordered moment per Mn ion is 0.5 μ_B, whereas a value of ∼3 μ_B would be expected for full long-range order of all spins. No change in the magnetic scattering is observed around the $T_F = 22$ K transition, confirming that this is most likely due to short-range spin freezing, although further neutron studies and AC magnetic susceptibility and μSR experiments will be useful in characterizing this state more fully.

Further insights into the magnetism of $Ba_5Sb_{1-x}Mn_{4+x}O_{15-\delta}$ may be obtained from subtle lattice responses to the spin correlations that may indicate the sites involved. No bulk magnetostrictions are evident for the hexagonal lattice parameters and cell volume, which show a normal thermal expansion behavior (Figure 10). The temperature dependencies of the Mn−O and Mn−Mn distances are shown in Figure 11. The clearest change below T_M is a decrease in the Sb/Mn1−O2 distance, and there is also a slight decrease in the Mn2−O2 distance, although the *M*1−O2−*M*2 angle shows no discontinuity (Figure 12). The other bonds do not show anomalies at T_M. Hence, the structural response indicates that local correlations between Mn spins, when present at the disordered *M*1 site, and the neighboring Mn2 spins are the principal contribution to the order occurring below T_M. No structural anomalies are evident at the $T_F = 22$ K spin freezing transition.

The magnetic order and frustration arise from the partial occupancy of Mn^{3+} at the *M*1 sites. The dominant magnetic superexchange interactions are associated with

(25) Yin, C.; Li, G.; Lin, J.; Attfield, J. P. *Chem. Asian J.* **2009**, *4*, 969.

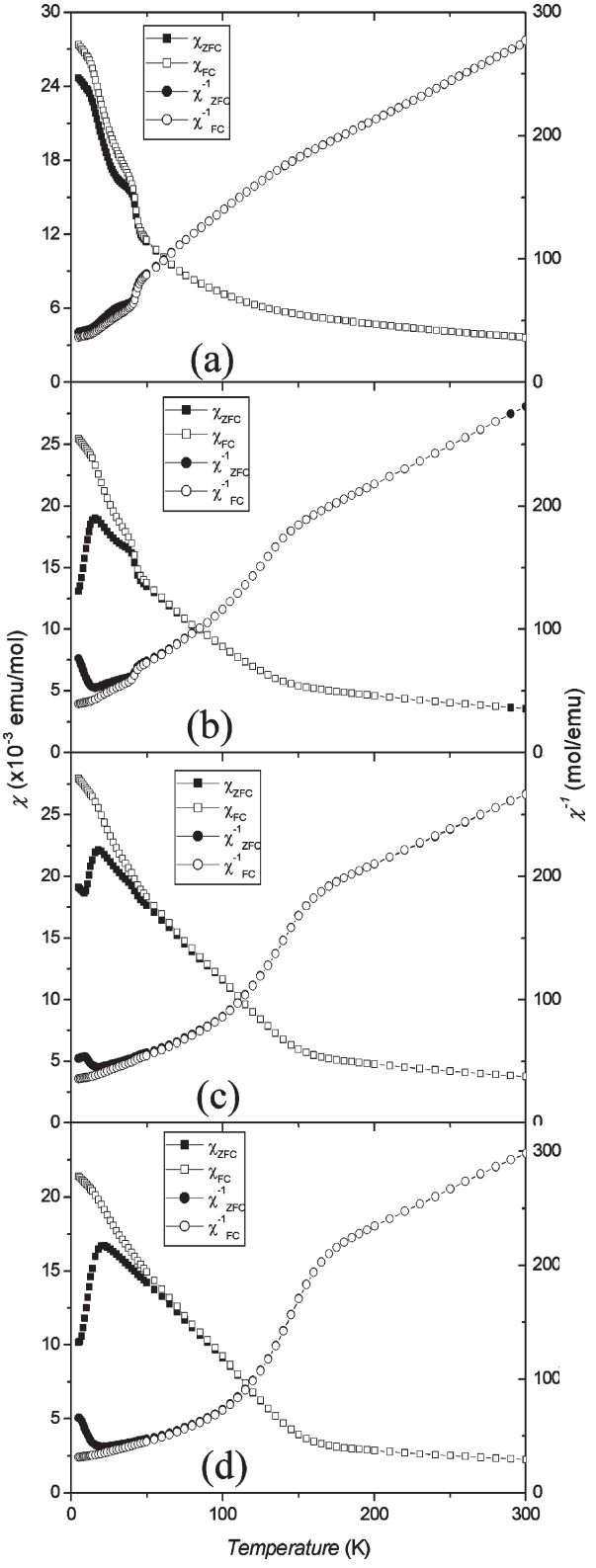

Figure 5. Molar magnetic susceptibility χ and inverse molar magnetic susceptibility χ^{-1} vs temperature for $Ba_5Sb_{1-x}Mn_{4+x}O_{15-\delta}$ samples with nominal x values of (a) 0.24, (b) 0.28, (c) 0.32, and (d) 0.36. Empty and filled symbols show field cooling (FC) and zero-field cooling (ZFC) data, respectively.

the $M1-O-M2$ connections, as these are the only near-linear bridges in the 10H structure type (see Table 2 and Figure 4). The hexagonal average lattice symmetry is incompatible with long-range orbital order, but when

Table 3. Magnetic Ordering and Weiss Temperatures and Effective Paramagnetic Moments per Mn Ion from Susceptibility Measurements on Four $Ba_5Sb_{1-x}Mn_{4+x}O_{15-\delta}$ Samples

x	T_F (K)	T_M (K)	θ (K)	μ_{eff} (μ_B)
0.24	13	129	−133	3.55
0.28	16	147	−143	3.56
0.32	18	160	−172	3.77
0.36	22	167	−164	3.53

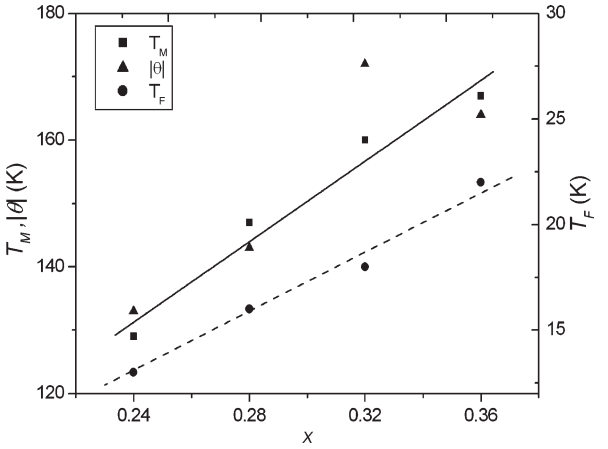

Figure 6. Plots of the magnetic ordering and Weiss temperatures vs the nominal Mn content x for $Ba_5Sb_{1-x}Mn_{4+x}O_{15-\delta}$.

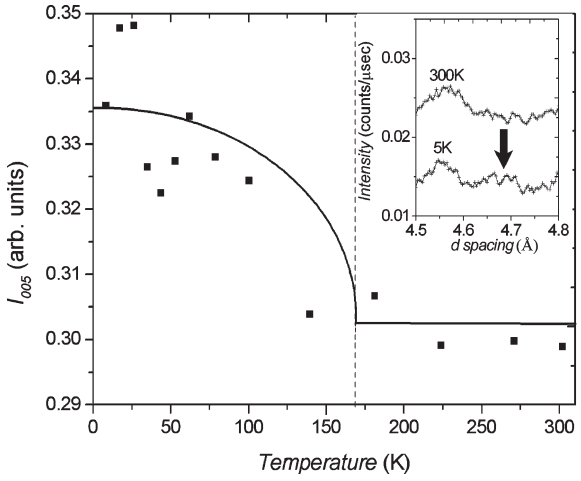

Figure 7. Temperature variation of the (005) magnetic neutron diffraction intensity for $Ba_5Sb_{1-x}Mn_{4+x}O_{15-\delta}$ ($x = 0.36$). The errors in the intensities are approximately ±0.015 arbitrary units. The inset shows the presence of this peak at 5 K (arrow) but not at 300 K.

Mn^{3+} ions are present at the $M1$ sites, local orbital order with respect to the Mn^{3+} and Mn^{4+} ions at the six neighboring $M2$ sites is likely in such a highly connected manganite network. This gives rise to a mixture of strong ferromagnetic and antiferromagnetic Mn1−O−Mn2 interactions (both types are found in long-range orbitally ordered and spin-ordered manganites such as $LaMnO_3$ and $La_{0.5}Ca_{0.5}MnO_3$[26]). Diamagnetic Sb^{5+} at the $M1$ sites introduces weaker antiferromagnetic Mn2−O−Sb−O−Mn2 exchange interactions. Hence, at T_M the

(26) Dagotto, E.; Hotta, T.; Moreo, A. *Phys. Rep.* **2001**, *344*, 1.

dominant order is within the $M2-M1-M2$ slabs according to the local exchange interactions described above.

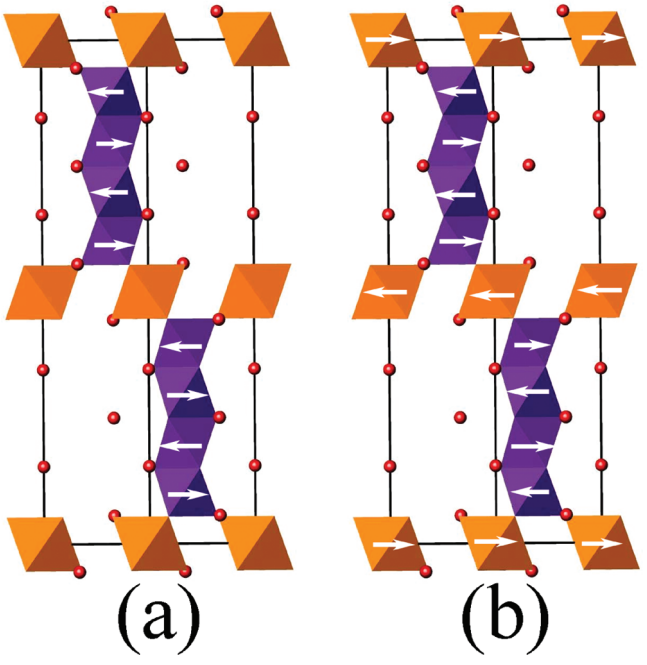

Figure 8. Two idealized models for magnetic order in $Ba_5Sb_{1-x}Mn_{4+x}O_{15-\delta}$, either of which can account for the (005) magnetic neutron diffraction intensity.

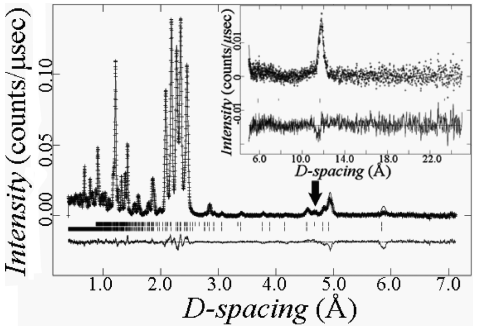

Figure 9. Fitted time-of-flight neutron diffraction profile of $Ba_5Sb_{1-x}Mn_{4+x}O_{15-\delta}$ ($x = 0.36$) at 5 K, with long d values from the low-angle detector bank shown in the inset. The (005) magnetic diffraction peak is denoted with an arrow.

The presence of a significant proportion of Mn at the $M1$ sites in $Ba_5Sb_{1-x}Mn_{4+x}O_{15-\delta}$ appears to be essential, as no magnetic order was observed in the 10H In- and Sn-doped analogues that contain mainly diamagnetic cations at $M1$. In addition, T_M increases proportionately with the excess Mn content, x, as discussed below. Order between successive slabs is via the Mn2−Mn3−Mn3−Mn2 tetramer clusters of face-sharing octahedra in which weaker antiferromagnetic interactions tend to result in the antiparallel alignment of neighboring spin layers, so that some net order can be observed by neutron diffraction. When the two terminal Mn2 spins are held parallel due to the local constraints of their Mn2−O−$M1$ interactions, spin order in the tetramer is frustrated, and this may lead to the dynamic ferro- or ferrimagnetic correlations that augment the susceptibility below T_M.

Long-range magnetic ordering transitions are usually suppressed when a material is doped with a nonmagnetic element, and these may evolve into a spin freezing transition at high dopings. However, the evolution of magnetism in $Ba_5Sb_{1-x}Mn_{4+x}O_{15-\delta}$ is unconventional in that two transitions with the characteristics of frustrated spin freezing and unfrustrated long-range order are observed over all available compositions. The characteristic magnetic temperatures (Table 3) show several simple physical behaviors. The frustration indices for the freezing transitions ($f_F = |\theta|/T_F$) lie in the range of 7−10, indicating highly frustrated magnetism. The freezing temperatures show an approximate $T_F \propto x$ variation, although the range of available compositions ($0.24 < x < 0.36$) does not allow other, nonlinear dependencies to be excluded. Monotonic $T_F \sim x$ variations are often observed when x represents the concentration of a magnetic dopant in a nonmagnetic host, e.g., for binary metallic spin glasses[27] or for the doping of Mn into metallic 6H $Ba_{0.7}Sr_{0.3}Ru_{1-x}Mn_xO_3$.[25] However, it is remarkable that a $T_F \propto x$ variation is observed in $Ba_5Sb_{1-x}Mn_{4+x}O_{15-\delta}$, where 80% of the possible cation sites are already occupied by magnetic cations and x represents the partial occupation of the remaining 20%. This further demonstrates that

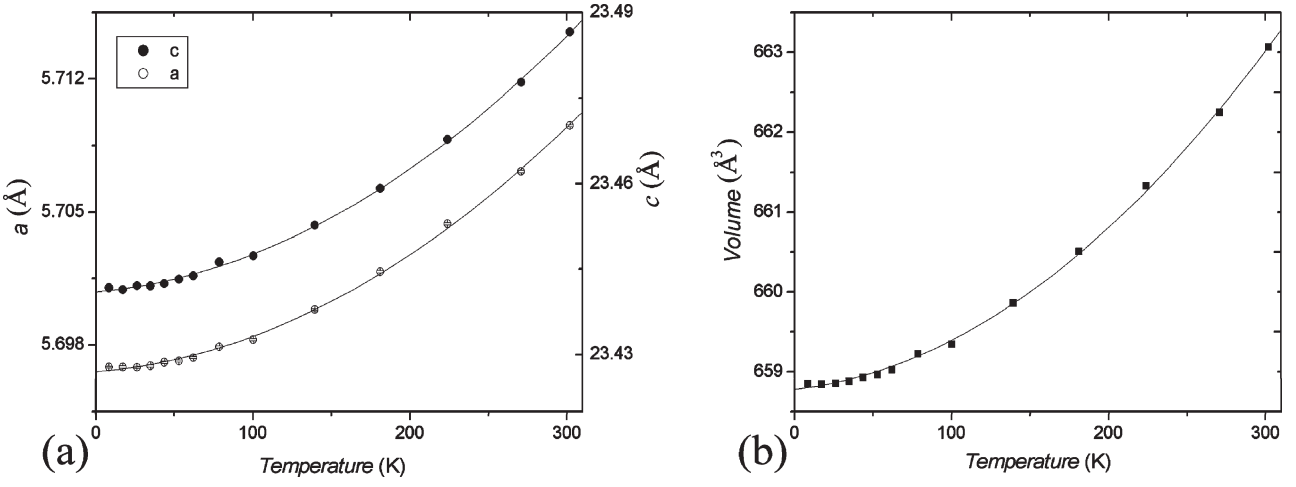

Figure 10. Variations of (a) lattice parameters and (b) cell volume with temperature for $Ba_5Sb_{0.64}Mn_{4.36}O_{15-\delta}$ with temperature.

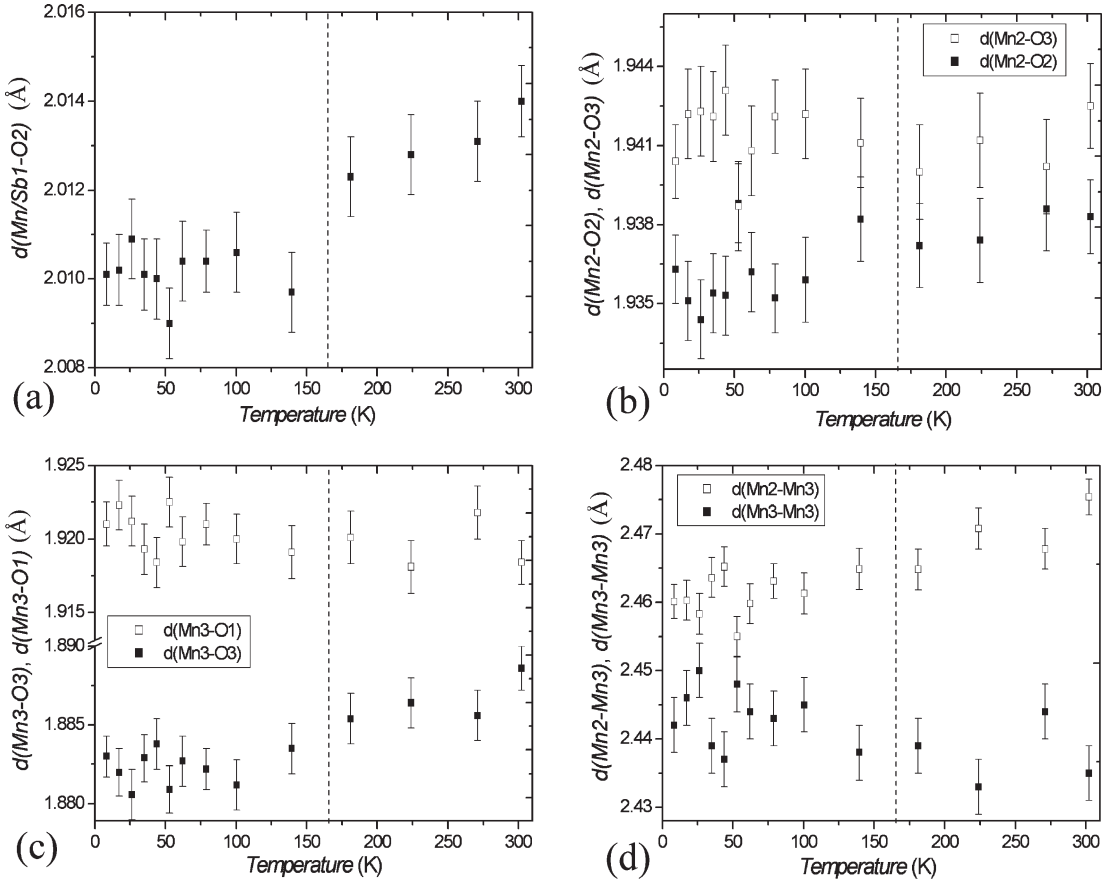

Figure 11. Temperature dependences of interatomic distances for $Ba_5Sb_{0.64}Mn_{4.36}O_{15-\delta}$: (a) Mn1/Sb1−O, (b) Mn2−O, (c) Mn3−O, and (d) Mn−Mn distances. The broken line shows the T_M = 167 K long-range magnetic ordering transition.

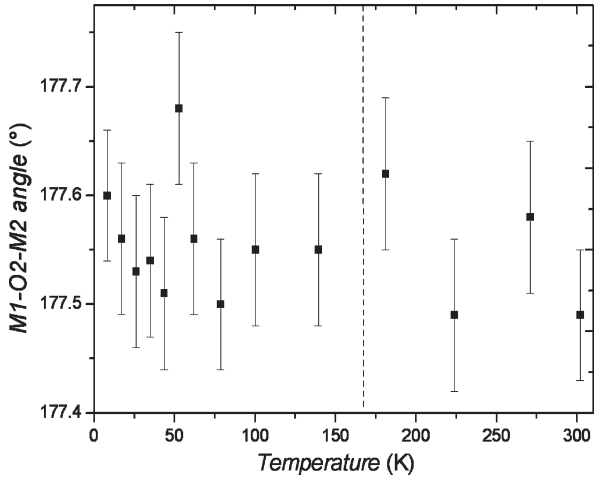

Figure 12. Temperature dependences of the $M1-O2-M2$ angle for $Ba_5Sb_{0.64}Mn_{4.36}O_{15-\delta}$. The dashed line shows the T_M = 167 K long-range magnetic ordering transition.

occupancy of the $M1$ sites by magnetic cations in the 10H form is key to establishing magnetic order.

It is also remarkable that the frustration index for the long-range spin ordering transition ($f_M = |\theta|/T_M$) is very close to unity for all $Ba_5Sb_{1-x}Mn_{4+x}O_{15-\delta}$ compositions (f_M values from Table 3 lie between 0.97 and 1.08). An f_M value of 1 is normally associated with unfrustrated spin order in simple three-dimensional magnetic lattices. The hypothetical $x = 1$ limiting composition of $Ba_5Sb_{1-x}Mn_{4+x}O_{15-\delta}$ would be likely to show essentially unfrustrated long-range spin order in Figure 8b at $T_M \approx 250$K, as similar antiferromagnetic orderings occur at 230−260 K in four other $BaMnO_{3-\delta}$ polymorphs.[5] Dilution of this order by Sb reduces T_M and introduces competing spin−spin interactions as described above, so the preservation of the $f_M \approx 1$ value for the transition even as the ordered moment becomes very small and the transition broadens (see Figure 5a for $x = 0.24$) is very unconventional. A possible explanation is that the frustration of competing interactions, which tend to give f_M values of >1, is accidentally compensated by the presence of significant, unfrustrated ferromagnetic interactions that promote f_M values of <1. Such locally cooperative networks of ferromagnetic and antiferromagnetic Mn−O−Mn interactions can arise from local Mn charge and orbital ordering, which occurs over long length scales in cubic manganites such as $La_{0.5}Ca_{0.5}MnO_3$. However, this compensation over all the $Ba_5Sb_{1-x}Mn_{4+x}O_{15-\delta}$ compositions appears to be very coincidental, and further studies of magnetic order as a function of x and using local probes will be needed to account more fully for the spin ordering phenomena.

4. Conclusions

Our results demonstrate that a new $Ba_5Sb_{1-x}Mn_{4+x}O_{15-\delta}$ solid solution can be prepared over the $0.24 \leq$

(27) Shegelski, M. R. A.; Geldart, D. J. W. *Phys. Rev. B* **1992**, *46*, 2853.

$x \leq 0.36$ range for samples fired at 1300 °C in air. It has a 10H perovskite structure with a well-defined distribution of cations, charge states, and oxygen vacancies over the available sites represented by the formula $Ba_5(Sb1^{5+}_{1-x}Mn1^{3+}_{x})(Mn2^{4+}_{0.5+x-\delta}Mn2^{3+}_{0.5-x+\delta})_2(Mn3^{4+})_2O_{15-\delta}$. The partial occupation of the $M1$ sites by Mn is notable as these interconnect the linear Mn2−Mn3−Mn3−Mn2 spin tetramers and result in magnetic ordering phenomena that were not observed in In- and Sn-doped analogues where $M1$ sites contain few or no Mn ions.

$Ba_5Sb_{1-x}Mn_{4+x}O_{15-\delta}$ solid solutions are Curie−Weiss paramagnets at high temperatures and show two magnetic transitions. The upper transition at $T_M \approx |\theta|$ corresponds to the formation of ferro- or ferrimagnetic clusters and the ordering of a small long-range antiferromagnetic component. Freezing of the magnetic clusters is observed at lower T_F temperatures that vary directly with the amount of Mn at the $M1$ sites, x.

Acknowledgment. This work is supported by the National Natural Science Foundation of China (Grant 20771008), EPSRC, and the Leverhulme Trust.